Polyaniline Nanocoating on the Surface of Layered $Li[Li_{0.2}Co_{0.1}Mn_{0.7}]O_2$ Nanodisks and Enhanced Cyclability as a Cathode Electrode for Rechargeable Lithium-Ion Battery

Docheon Ahn,[†,‡] Yang-Mo Koo,[‡] Min Gyu Kim,[†] Namsoo Shin,[†] Jaehun Park,[†] Junho Eom,[§] Jaephil Cho,[§] and Tae Joo Shin*[,†]

Pohang Accelerator Laboratory, Pohang 790-784, Republic of Korea, Department of Materials Science and Engineering, POSTECH, Pohang 790-784, Republic of Korea, and School of Energy Engineering, UNIST, Ulsan 689-798, Republic of Korea

Received: October 5, 2009; Revised Manuscript Received: December 9, 2009

The surfaces of layer-structured $Li[Li_{0.2}Co_{0.1}Mn_{0.7}]O_2$ nanodisks were nanocoated with polyaniline and examined by SEM and TEM studies, via the chemical oxidative polymerization of aniline in an acid medium for 10 min—Mn^{4+} ions in the pristine lithium manganese oxides acted as oxidants. During this reaction, the crystal structure of the pristine nanodisks was retained, and the XRD patterns showed no evidence of H^+ exchange with the Li^+ located between the manganese oxide layers. The nanocoated polyaniline was in the low molecular weight of base states, and the majority (~70%) was complexed with $Li[Li_{0.2}Co_{0.1}Mn_{0.7}]O_2$ nanodisks, as shown by UV−vis and FT-IR spectroscopic analysis. By application of nanocoated polyaniline nanodisks as the cathode material, the discharge capacity was improved by about 15%. Furthermore, the cyclability was enhanced with almost no change in discharge capacity being detected at extended cycle numbers, while that of pristine nanodisks showed a tendency to continually decrease as the number of cycles increased. Results from the present study suggest that a well-controlled polyaniline nanocoating, particularly formed with the aid of pristine metal oxides as oxidants for polymerization, can act as a potential buffer layer between electrodes and electrolytes, which makes this a promising method for the reducing/protection of continuous structural distortion that occurs during extended charge−discharge cycling.

Introduction

Rechargeable lithium-ion batteries consisting of a nanostructured cathode of lithium transition metal oxides are known to provide excellent electrochemical performance: high energy storage capacity and fast charge−discharge kinetics due to a large surface area for faradaic reaction and a short distance for mass and charge diffusion, as well as the added freedom for volume change that accompanies lithium-ion intercalation and discharge.[1–4] However, the structural transformation of active materials and the instability of the electrode capacity caused by the dissolution of transition metals in electrolyte solutions can cause problems.[5]

Intercalation of guest organic molecules (or conductive polymers) into the layered nanostructure of manganese oxides has been widely studied in recent years in the pursuit of unique functions that are unachievable through the use of conventional manganese oxides.[6–12] However, since layered manganese oxide has a higher charge density in the interlayer than other layered materials such as vanadium oxides, the intercalation process is known to be quite complex and difficult.[13] Recently, a simple method has been reported for poly(diallylmethylammonium chloride)[13] or polyaniline intercalation[14] into layered manganese oxides using a delamination−reassembly process, whereby the chemical oxidation polymerization of aniline occurs at the aqueous−organic interface while the oxidant MnO^{4-} is simultaneously reduced to form a manganese oxide precipitate. However, in general, decreases in the crystallinity of the inorganic components are often reported in conducting polymer−metal oxide composites prepared by oxidative polymerization in an acidic medium.[15,16] Using metal oxides as oxidants can sometimes result in no improvement of cyclability, although there is quite an improvement in capacity.[16]

A controlled conducting polymer nanocoating on the surface of transition metal oxides can be an alternative solution for unwanted phase transformation and dissolution. As long as the original crystalline structure and crystallinity of metal oxides are preserved during oxidative polymerization in an acidic medium containing metal oxides as oxidants, a controlled polymer coating can reduce the dissolution of a transition metal ion and can supply structural stability during charge−discharge cycles, thus improving the cycle life of the cell. Although some researchers have reported the use of conducting polymer nanocoating on the surface of metal oxides,[17–19] to our knowledge, there have been few studies of a controlled polyaniline nanocoating using metal oxide oxidants and their effect on electrochemical performance. The aim of a nanocoating on the surface of active metal oxides is to inhibit the undesirable dissolution of transition metals and phase transformation during charge−discharge cycles, while fully utilizing all the advantages of nanostructured metal oxides and maintaining the original high-energy storage capacity.

It is noteworthy that while both $LiMnO_2$- and Li_2MnO_3-based oxides, such as $Li[Co_xLi_{(1/3-x/3)}Mn_{(2/3-2x/3)}]O_2$, have layered structures, they show different electrochemical behaviors during charge−discharge cycling. It is well-known that, during cycling, a structure transformation of $LiMnO_2$ occurs due to the intrinsic Jahn−Teller distortion of active Mn^{3+}, which results in capacity fading.[20,21] In the case of Li_2MnO_3-based oxides, however, the

* To whom correspondence should be addressed. Tel.: +82 54 2791166. Fax: +82 54 2791599. E-mail: stj@postech.ac.kr.
† Pohang Accelerator Laboratory.
‡ POSTECH.
§ UNIST.

10.1021/jp9095437
Published on Web 02/09/2010

electrolyte is oxidized in a 4.2−4.5 V potential range by O^{2-} species at the electrode surface, resulting in the generation of H^+ at the electrode surface.[22–25] Subsequently, the generated H^+ exchanges with Li^+ in the electrode causing the distortion of the MnO_6 octahedron in the Li_2MnO_3, which results in conversion of Li_2MnO_3 to a spinel-like phase upon extended cycling. Therefore, if a well-controlled nanocoating could act as a buffer layer at the surface of the electrode, then this kind of unwanted reaction between the electrode and electrolyte could be reduced, which could improve its cycling stability.

In the present study, layered $Li[Li_{0.2}Co_{0.1}Mn_{0.7}]O_2$ nanodisks were synthesized by hydrothermal treatment, and their surface was uniformly nanocoated with polyaniline via the chemical oxidative polymerization of aniline in an acid medium, in which pristine metal oxide nanodisks acted as oxidants. Their electrochemical performance, charge−discharge capacity and cyclability, was measured to examine the effect of nanocoating on a metal oxide electrode. When the nanocoated metal oxides were used as the cathode material, the discharge capacity was enhanced by ∼15% and cyclability was improved to show little change in discharge capacity over 20 cycles, while that of pristine nanodisks showed a continuous decreasing trend with increasing cycles.

Experimental Section

Pristine $Li[Li_{0.2}Co_{0.1}Mn_{0.7}]O_2$ Nanodisks (Pristine NDs). Co-doped manganese oxide powder ($Co_{0.1}Mn_{0.9}O_2$), prepared by ion exchange from K-birnessite powder ($K_{0.32}MnO_2$),[26,27] was mixed with $LiNO_3 \cdot H_2O$ at a 1:5 molar ratio in 20 mL of distilled water and was transferred to a hydrothermal bomb reactor (Parr, U.S.) and then annealed at 200 °C for 24 h. The sample was then centrifuged, washed with distilled water, and dried in an oven at 70 °C for 1 day. As a result, a nanorod-shaped powder was acquired, and no phase transformation was observed during this hydrothermal treatment, which was confirmed by FE-SEM images and XRD patterns. This powder sample was mixed with $LiOH \cdot H_2O$ at a 1:5 molar ratio in 20 mL of distilled water and hydrothermally treated again at 200 °C for 5 h in a reactive bomb. The sample was then centrifuged, washed with distilled water, and dried in an oven at 70 °C for 1 day. During this second hydrothermal treatment, the nanorod-shaped powder was converted to a nanodisk-shaped one (pristine NDs), undergoing phase transformation from a birnessite to an α-$NaFeO_2$ structure, which was revealed by XRD analysis.

Polyaniline-Nanocoated $Li[Li_{0.2}Co_{0.1}Mn_{0.7}]O_2$ Nanodisks (PANI-Coated NDs). Polyaniline-nanocoated $Li[Li_{0.2}Co_{0.1}Mn_{0.7}]O_2$ nanodisks (PANI-coated NDs) were prepared by chemical oxidative polymerization in the presence of hydrochloric acid (HCl) with the aid of pristine nanodisks as oxidants. The polymerization procedure was as follows. An acidic aniline monomer solution was prepared by mixing 0.1 mL of aniline monomer with 0.44 mL of HCl (35%) in 60 mL of aqueous solution with stirring at r.t. for 1 h. An aqueous $Li[Li_{0.2}Co_{0.1}Mn_{0.7}]O_2$ nanodisk solution was prepared by the dispersion of 0.2 g of the $Li[Li_{0.2}Co_{0.1}Mn_{0.7}]O_2$ nanodisk sample in 50 mL of distilled water with stirring at r.t. for 30 min. Next, the acidic aniline monomer solution was mixed with the aqueous $Li[Li_{0.2}Co_{0.1}Mn_{0.7}]O_2$ nanodisk solution with stirring for simultaneous polymerization and nanocoating. After reaction for 10 min, a dark blue-colored solution was obtained. This solution was filtered using a glass filter, and then it was washed with distilled water and ethanol until the filtrate became colorless, followed by drying in an oven at 70 °C for 1 day. For comparison, a polyaniline nanocomposite with $Li[Li_{0.2}Co_{0.1}Mn_{0.7}]O_2$ nanodisks (PANI-composite NDs) was prepared using a 0.5 mL of aniline monomer and 0.88 mL of HCl (35%) for the aniline monomer solution and 0.2 g of $Li[Li_{0.2}Co_{0.1}Mn_{0.7}]O_2$ nanodisks for a nanodisk solution using the same method mentioned above. A bulk polyaniline sample (bulk PANI) was also prepared using a typical APS/pristine NDs/HCl system, where APS is ammonium persulfate $[(NH_4)_2S_2O_8]$.

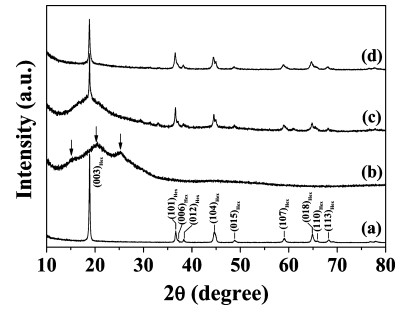

Figure 1. Synchrotron powder X-ray diffraction patterns of (a) pristine $Li[Li_{0.2}Co_{0.1}Mn_{0.7}]O_2$ NDs, (b) bulk PANI powder, (c) PANI-composite NDs, and (d) PANI-coated NDs. Arrows in (b) show regular periodicity parallel and perpendicular to the polyaniline chains, suggestive of its low crystallinity.

Preparation of the Electrochemical Cells and the Performance Test. The cathode was developed by mixing pristine or polyaniline-nanocoated $Li[Li_{0.2}Co_{0.1}Mn_{0.7}]O_2$ nanodisks, super P carbon black (MMM, Belgium), and poly(vinylidene fluoride) binder (Solef) at a weight ratio of 65:20:15. The mixed slurry was cast onto Al foil, followed by drying at 130 °C for 1 h. Coin-type test cells (size 2016R) composed of a cathode, a Li metal anode, a microporous polyethylene separator, and an electrolyte (Cheil Ind., Korea; 1.03 M $LiPF_6$ in 3/3/4 vol % ethylene carbonate/diethylene carbonate/ethyl methyl carbonate) were prepared in a helium-filled glovebox. Electrochemical tests were performed using a MACCOR Series 4200 cycler. During this test, in order to investigate the polyaniline nanocoating effect on electrochemical behavior and electrolyte stability, the range for cutoff was fixed at 2.0−4.8 V for all cycles.

Results and Discussion

Powder X-ray Diffraction. Figure 1 shows the synchrotron powder X-ray diffraction (XRD) patterns of pristine NDs, bulk PANI, PANI-composite NDs, and PANI-coated NDs, respectively.[28] In order to accurately determine the profile shape function and lattice parameters of the pristine NDs, prior to Rietveld refinement analysis, each XRD pattern was fitted using a whole-pattern profile matching method. The system was modeled after the rhombohedral phase of an $R3\bar{m}$ space group, which is the isostructure of $LiCoO_2$ (α-$NaFeO_2$ structure). The lattice parameters of the pristine NDs obtained from the fit were $a = 2.8901(1)$ Å and $c = 14.1684(9)$ Å. Detailed peak indexing is shown in Figure 1a. Rietveld refinement[29] and induced-coupled plasma (ICP) atomic emission spectrometer (OPIMA 4300 DV, Perkin-Elmer) analysis confirmed that the pristine nanodisks had a lithium rich composition, $Li[Li_{0.2}Co_{0.1}Mn_{0.7}]O_2$.

The bulk PANI powder showed very weak reflections at $2\theta = 16.16°$, 20.28°, and 25.24° (as shown by the arrows in Figure 1b), which were attributed to the regular periodicity parallel and perpendicular to the polymer chains,[30–32] suggesting that this bulk PANI power was only partially crystalline. In Figure 1c, the PANI-composite NDs show the mixed XRD pattern of pristine NDs and bulk PANI, in which the intensity of the $(003)_{hex}$ reflection of pristine NDs was quite weakened and only

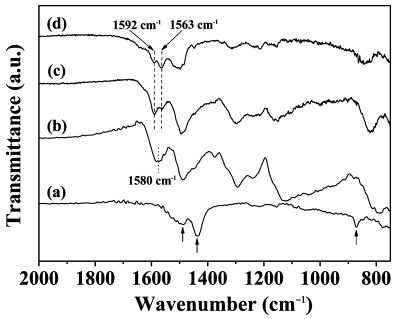

Figure 2. IR spectra of (a) pristine $Li[Li_{0.2}Co_{0.1}Mn_{0.7}]O_2$ NDs, (b) bulk PANI powder, (c) PANI-composite NDs, and (d) PANI-coated NDs. Arrows in (a) correspond to $\nu(CO_3^{2-})$ and $\delta(CO_3^{2-})$ vibrational bands of Li_2CO_3 impurity. The characteristic Q-band at 1580 cm^{-1} is split into two peaks at 1592 and 1563 cm^{-1} for PANI-composite NDs and PANI-coated NDs.

an amorphous-like XRD pattern was found resulting from polyaniline. The XRD pattern of the PANI-coated NDs intensity of the $(003)_{hex}$ reflection, as with PANI-composite NDs, was also decreased compared to other diffraction peaks maintaining the original crystal structure of pristine nanodisks. For instance, the intensity ratio of the $(003)_{hex}$ reflection:$(101)_{hex}$ reflection was 7.8:1 for pristine NDs but 2.4:1 for PANI-coated NDs, suggesting that either the preferred orientation along the *c*-axis was disturbed or a possibility that the surface was affected during oxidative polymerization by the rearrangement of elements. Characteristically, the diffraction peaks of polyaniline crystals were not observed for PANI-coated NDs possibly due to the amorphous polyaniline coating on the nanodisks.

Since the chemical oxidative polymerization was aided by Mn^{4+}, some compositional change of $Li[Li_{0.2}Co_{0.1}Mn_{0.7}]O_2$ was expected. The change, however, was expected to be very small because this reaction occurred on the surface of the nanodisks within a very short reaction time (10 min) and a catalytic amount of Mn^{4+} was used. Chemical oxidative polymerization of aniline carried in acidic medium can cause a proton exchange reaction. However, there was no evidence of H^+ exchange with the Li^+ located between the manganese oxide layers, as seen from the (003) reflection in the XRD pattern, which suggested that 10 min of reaction time was too short to cause such a proton exchange effectively, particularly within the layers. Furthermore, there was little or no chance for proton exchange on the surface, because the majority of Li^+ was located within manganese oxide layers and once polyaniline nanocoating was formed on the electrode surface, any proton exchange on it would have been suppressed.

FT-IR Spectroscopy. To further examine the polyaniline nanocoating, FT-IR spectroscopic studies were conducted. In the IR spectrum of pristine NDs, three characteristic vibrational bands at 1485, 1430, and 870 cm^{-1} were detected, as shown in Figure 2a (see arrows). The first two bands corresponded to CO_3^2 stretching and the last to CO_3^{2-} bending vibration from an Li_2CO_3 impurity,[33,34] the structure of which was not observed in the XRD pattern possibly because of its trace amount and weak X-ray scattering density.

The bulk PANI showed two intense vibration bands at approximately 1580 and 1490 cm^{-1} (Figure 2(b)), which corresponded to characteristic C═C stretching vibrations of the quinoid (Q-band) and benzenoid ring (B-band) of a polyaniline base, respectively.[35,36] In this study, as mentioned in the Experimental Section, the bulk polyaniline sample (bulk PANI) was prepared using an APS/pristine NDs/HCl system. Similar IR spectra for bulk PANI can be found elsewhere.[37–40]

It should be noted here that the Li_2CO_3 impurity, found in pristine NDs, seemed to be removed during the oxidative polymerization in an acid medium because characteristic $\nu(CO_3^{2-})$ and $\delta(CO_3^{2-})$ vibrational bands were not observed in the IR spectrum of PANI-coated NDs and PANI-composite NDs. In Figure 2c and d, specifically, the Q-band was split into two vibrational bands at 1563 and 1592 cm^{-1}, showing differing absorption ratios for PANI-composite NDs and PANI-coated NDs. For example, the absorbance ratios of two peaks, $A_{1563cm-1}/A_{1592cm-1}$, corresponding to absorbance at 1563 and 1592 cm^{-1}, were 0.7 and 2.4 for PANI-composite NDs and PANI-coated NDs, respectively (see Figure S1 in the Supporting Information). When a PANI base is properly doped, the Q-band is known to shift to a lower wavenumber in the range of 1560−1570 cm^{-1}.[35,36,41] In the present study, however, there was no proper doping procedure during the synthesis. Furthermore, UV−vis absorption spectra of PANI-composite NDs and PANI-coated NDs showed no characteristic polyaniline in the form of a doped emeraldine salt (see Figure S2 in the Supporting Information). Therefore, the vibrational band at 1563 cm^{-1} can be interpreted as the band from some specific interactions between the PANI base and the metal oxide nanodisks.

Carbonyl stretching bands are reported to be quite sensitive to conjugated conformations[42,43] or to specific interactions, such as hydrogen bonding[44] and an acid−base interaction.[45] As the conjugated conformation, or specific interaction, was more enhanced, it shifted more to a lower wavenumber. For example, the "true" isolated "free" and "fully hydrogen-bonded" carbonyl groups showed stretching vibrational bands at around 1740 and 1700 cm^{-1}, respectively, while "interassociated" carbonyl bands appeared at 1728 cm^{-1}.[44] If this concept is applied to the characteristic Q-band split at 1593, 1580, and 1563 cm^{-1}, they can be interpreted as a PANI base with slight, moderate, and high interactions with other PANI molecules or metal oxide nanodisks, respectively. Since bulk PANI, showing a Q-band at 1580 cm^{-1}, is only characteristic of an interaction between PANI molecules, the explanation of a Q-band shift to 1563 cm^{-1} must have a specific strong interaction between PANI molecules and metal oxide nanodisks, such as hydrogen-bonding[46] or charge-transfer complexing. Here, polyaniline had an increased possibility for the formation of a charge-transfer complex because metal oxides act as oxidants that are required for the initiation and propagation of polymerization, which may be the driving force for PANI nanocoating under specific conditions, such as those found in the present study. As mentioned above, PANI-composite NDs showed a smaller value for $A_{1563cm-1}/A_{1592cm-1}$ compared with that of PANI-coated NDs, which is indicative of a higher portion of "free or less-interacted" PANI base. Conclusively, when the Q-band is split into two peaks, an absorbance ratio of 1563 and 1592 cm^{-1} indicates a free and complexed PANI base.

At this point, it is important to discuss why only the PANI base was observed for PANI-composite NDs and PANI-coated NDs in the present study. During the chemical synthesis of PANI, the radical cations of aniline in a pernigraniline state, which can be reduced to an emeraldine oxidation state when excess monomer is present, are known to first be formed, and subsequently adsorbed, as it is polymerized leading to the growth of polymer chains.[47] Therefore, an especially small amount of aniline monomer (∼1 mmol aniline) dissolved in 0.1 M HCl with a short reaction time (10 min) at r.t. may result in a relatively low molecular weight[48] for PANI base.

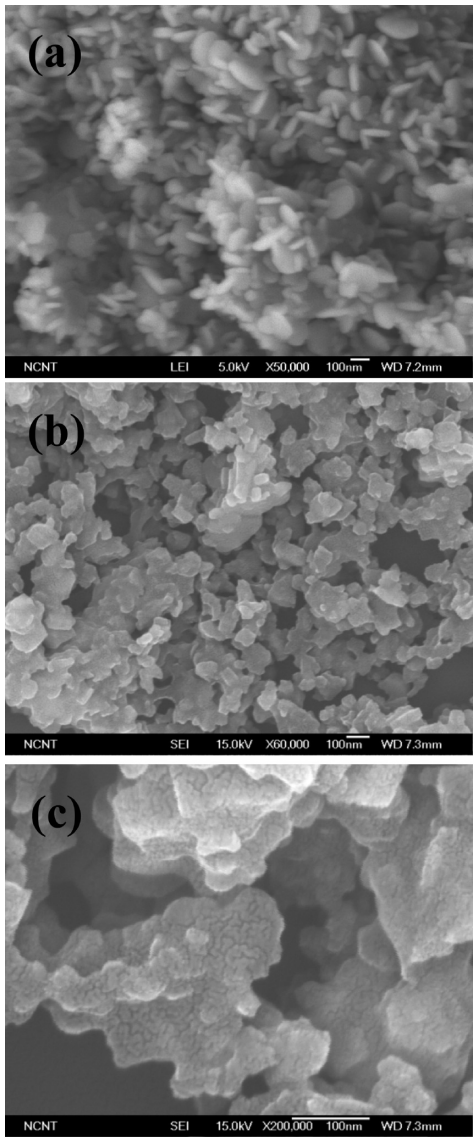

Figure 3. SEM images of (a) pristine $Li[Li_{0.2}Co_{0.1}Mn_{0.7}]O_2$ NDs and (b) PANI-coated NDs and (c) high-resolution SEM image (×60 000) of PANI-coated NDs. Surface morphology of PANI nanocoating with uniform mosaicity is clearly seen in (c).

Scanning Electron Microscopy (SEM) and Transmission Electron Microscopy (TEM). Since the effect of PANI nanocoating on the surface of pristine NDs was a major concern in the present study, pristine NDs and PANI-coated NDs were further investigated by SEM and TEM, the results of which are shown in Figure 3. The SEM image of the pristine NDs clearly showed individually dispersed nanodisks of 100−150 nm in diameter and 15−25 nm in thickness (see Figure 3a). After undergoing oxidative polymerization and a simultaneous coating process in acidic medium, pristine NDs seemed to lose their dispersed morphological features and piled upon one another to then be linked (Figure 3b). The edges of the PANI-coated NDs had a trimmed appearance, which was suggestive of the dismutation of a nanodisk in an acidic medium according to the following reaction: $2Mn^{+3} \rightarrow Mn^{4+}$ (bulk) + Mn^{2+} (solution).[49] Figure 3c shows the high-resolution SEM image (×60 000) of PANI-coated NDs, in which a characteristically uniform mosaic surface morphology is clearly observed. It is our contention that the origin of that morphology resulted from the nanocoating of the polyaniline, because the SEM image of pristine NDs treated with 0.1 M HCl for 10 min, without an aniline monomer, showed almost the same surface morphology as pristine NDs (see Figure S3 in the Supporting Information).

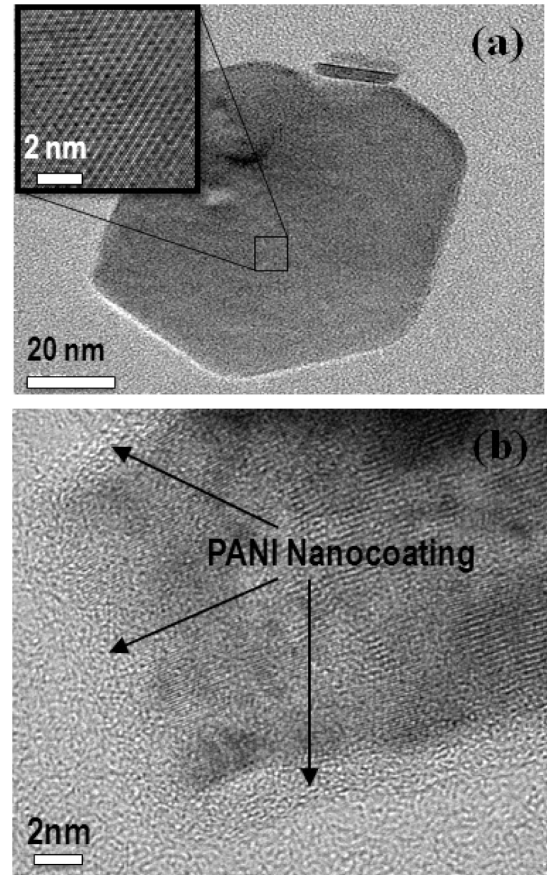

Figure 4. TEM images of (a) pristine $Li[Li_{0.2}Co_{0.1}Mn_{0.7}]O_2$ NDs and (b) PANI-coated NDs. Inset of (a) displays the hexagonal crystal structure of pristine $Li[Li_{0.2}Co_{0.1}Mn_{0.7}]O_2$ NDs. A PANI nanocoating layer approximately 2 nm thick is clearly seen in (b).

Based on both the IR results of Li_2CO_3 impurity removal during oxidative polymerization and the uniform mosaic surface morphology formed via oxidative polymerization, it can be suggested that Li_2CO_3 impurities, mostly formed on the surface and/or at the edge region of nanodisks, were removed, and the surface regions were nanocoated with low molecular weight polyaniline via oxidative polymerization. These cleaning and coating roles are quite important for the electrochemical performance of lithium-ion rechargeable batteries, particularly with regard to capacity fading, because structural (microstructural) stability[50,51] and surface stability[52,53] are proposed as the cause for capacity fade. Therefore, the surface cleaning and nanocoating that results from the oxidative polymerization and concurrent nanocoating processes can enhance surface stability, thereby improving cyclability.

To better understand the nanostructure of pristine NDs and PANI-coated NDs, HR-TEM images were measured. A TEM image of pristine NDs, presented in Figure 4a, showed that the basic crystalline morphology was that of a hexagonal-shaped disk composed of a hexagonal crystal structure (see inset of Figure 4a), which is consistent with the XRD data shown in Figure 1a. The lattice fringes of the nanodisks with a uniform PANI nanocoating layer formed at the edge are clearly shown by the arrows in Figure 4b. The layer thickness at the edge of the nanodisks was estimated to be about 2 nm.

Electrochemical Performance. To examine the effects of PANI nanocoating, electrochemical performance in the range

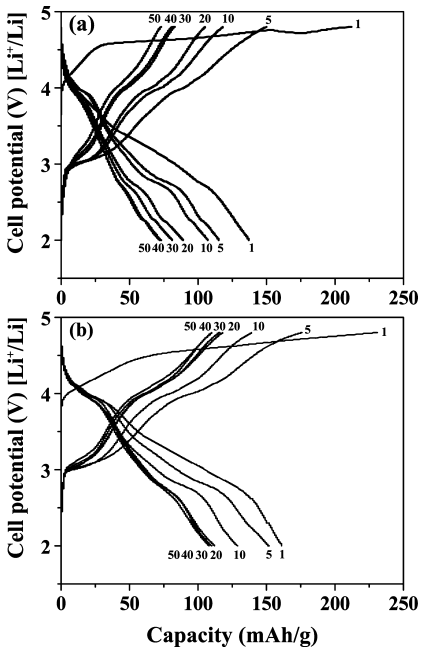

Figure 5. Charge−discharge curves of (a) pristine NDs and (b) PANI-coated NDs.

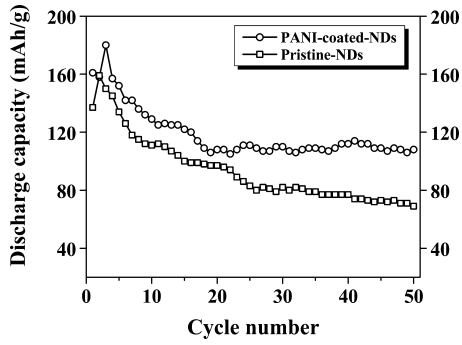

Figure 6. Cycle performances of pristine $Li[Li_{0.2}Co_{0.1}Mn_{0.7}]O_2$ NDs (□) and PANI-coated NDs (○) measured at 12 mA/g in the 2−4.8 V range.

of 2.0−4.8 V was evaluated for both pristine NDs and PANI-coated NDs used as positive electrodes for rechargeable lithium-ion batteries. The charge−discharge curves of pristine NDs and PANI-coated NDs are shown in Figure 5. For both samples, a long plateau was observed at 4.4−4.6 V in the first charge curve, respectively. A similar irreversible voltage plateau during the first charge process has been reported in Li_2MnO_3-based oxides.[54–56] At the first cycle, the charge and discharge capacities of pristine NDs were 212 and 137 mAh/g, respectively, showing a 65% coulombic efficiency, while those of PANI-coated NDs were 231 and 161 mAh/g, respectively, showing a 70% coulombic efficiency.

Figure 6 shows the plot of the cycle number vs discharge capacity of test cells acquired from charge−discharge curves, describing cycle performances of pristine NDs and PANI-coated NDs, respectively. Both pristine NDs and PANI-coated NDs showed a similar declining trend in discharge capacity of up to 19 cycles, while the PANI-coated NDs retained about 15% higher discharge capacity than that of the pristine NDs. Above 20 cycles, the discharge capacity of the pristine NDs continuously decreased until it had reached ∼70 mAh/g at the 50th cycle. The PANI-coated NDs, however, had retained their value at ∼110 mAh/g by the 50th cycle, which was ∼57% higher than that of the pristine NDs. In general, nanostructured positive electrodes prepared by low-temperature routes, such as with low-temperature hydrothermal synthesis, are known to easily react with electrolytes due to their large surface area, which leads to poor cycling stability.[1,5] Therefore, it is possible that pristine NDs also undergo these unwanted reactions with electrolytes during cycling, which results in poor cycle stability. On the other hand, as shown in Figure 6, PANI-coated NDs show good cycle stability above 20 cycles. This suggests that by reducing the contact areas between positive electrodes and electrolytes, PANI nanocoating acts as a stabilizing buffer layer that prevents further unwanted reactions of nanodisks during higher cycling. As a result, controlled PANI nanocoating on metal oxides is an effective means of reducing secondary reactions such as the dissolution of transition metals, electrolysis of water, and other redox reactions. In the present study, controlled PANI nanocoating on metal oxides provided structural stability during charge−discharge cycles, and thus improved the cyclability of a cell.

Conclusions

We have demonstrated that polyaniline nanocoating, prepared by simple oxidative polymerization, effectively enhanced the cyclability of a layered $Li[Li_{0.2}Co_{0.1}Mn_{0.7}]O_2$ nanodisk. Coated polyaniline in the amorphous phase of a low molecular weight polyaniline base was complexed with metal oxide nanodisks. Although Mn^{4+} ions were used as oxidants during the polymerization of aniline in an acidic medium, the original crystalline structure and crystallinity of PANI-coated NDs were fairly well preserved. In the presence of nanocoated polyaniline on positive electrodes, test cells displayed good cycle stability in the range of 20−50 cycles with no decrease of discharge capacity, while pristine NDs showed a continuous decreasing cycle behavior within the same cycle range. These results suggest that the PANI nanocoating acted as a protection buffer layer for unnecessary secondary reactions in a rechargeable battery. It can be concluded that controlled polyaniline nanocoating of Li_2MnO_3-based cathode material is an effective alternative for improving the cycle life of a cell.

Acknowledgment. The authors acknowledge the help of Mi-Sook Kim, Na-Hyung Kim, and Ha Na Won, who provided enormous support for the basic experiments of metal oxides and polyaniline nanocoating. This work was supported by a Korea Science and Engineering Foundation (KOSEF) grant funded by the Korea government, the Ministry of Education, Science & Technology (MEST) No. 20090060053, and WCU (World Class University) program through the National Research Foundation of Korea funded by the Ministry of Education, Science and Technology.

Supporting Information Available: IR spectra of PANI-coated NDs and PANI-composite NDs (Figure S1), UV−vis absorption spectra of PANI-composite NDs and PANI-coated NDs (Figure F2), and high-resolution SEM image (×60 000) of pristine NDs treated with 0.1 M HCl for 10 min (Figure S3). This material is available free of charge via the Internet at http://pubs.acs.org.

References and Notes

(1) Wang, Y.; Cao, G. *Adv. Mater.* **2008**, *20*, 2251.
(2) Ji, X.; Lee, K. T.; Nazar, L. F. *Nat. Mater.* **2009**, *8*, 500.
(3) Kim, M. G.; Cho, J. *Adv. Funct. Mater.* **2009**, *19*, 1.
(4) Bruce, P. G.; Scrosati, B.; Tarascon, J.-M. *Angew. Chem., Int. Ed.* **2008**, *47*, 2930.
(5) Li, W.; Dahn, J. R. *J. Electrochem. Soc.* **1995**, *142*, 1742.

(6) Liu, Z. H.; Ooi, K.; Kanoh, H.; Tang, W. P.; Tomida, T. *Langmuir* **2000**, *16*, 4154.
(7) Gao, Q. M.; Giraldo, O.; Tong, W.; Suib, S. L. *Chem. Mater.* **2001**, *13*, 778.
(8) Omomo, Y.; Sasaki, T.; Wang, L. Z.; Watanabe, M. *J. Am. Chem. Soc.* **2003**, *125*, 3568.
(9) Wang, L. Z.; Takada, K.; Kajiyama, A.; Onoda, M.; Michiue, Y.; Zhang, L. Q.; Watanabe, M.; Sasaki, T. *Chem. Mater.* **2003**, *15*, 4508.
(10) Yang, X. J.; Makita, Y.; Liu, Z. H.; Sakane, K.; Ooi, K. *Chem. Mater.* **2004**, *16*, 5581.
(11) Kadoma, Y.; Uchimoto, Y.; Wakihara, M. *J. Phys. Chem. B* **2006**, *110*, 174.
(12) Fukuda, K.; Nakai, I.; Ebina, Y.; Tanaka, M.; Mori, T.; Sasaki, T. *J. Phys. Chem. B* **2006**, *110*, 17070.
(13) Liu, Z. H.; Yang, X. J.; Makita, Y.; Ooi, K. *Chem. Mater.* **2002**, *14*, 4800.
(14) Wang, Y.-G.; Wu, W.; Cheng, L.; He, P.; Wang, C.-X.; Xia, Y.-Y. *Adv. Mater.* **2008**, *20*, 2166.
(15) Lira-Cantu, M.; Gomez-Romero, P. *J. Electrochem. Soc.* **1999**, *146*, 2029–2033.
(16) Gemeay, A. H.; Mansour, I. A.; El-Sharkawy, R. G.; Zaki, A. B. *Eur. Polym. J.* **2005**, *41*, 2575.
(17) Wang, H.; Huang, K.; Zeng, Y.; Zhao, F.; Chen, L. *Electrochem. Solid State Lett.* **2007**, *10*, A199.
(18) Huang, C.-L.; Partch, R. E.; Matijevic, E. *J. Colloid Interface Sci.* **1995**, *170*, 275.
(19) Ayad, M. M.; Salahuddin, N.; Shenashin, M. A. *Synth. Met.* **2004**, *142*, 101.
(20) Shao-Horn, Y.; Hackney, S. A.; Armstrong, A. R.; Bruce, P. G.; Gitzen-danner, R.; Johnson, C. S.; Thackeray, M. M. *J. Electrochem. Soc.* **1999**, *146*, 2404.
(21) Ammundsen, B.; Paulsen, J. *Adv. Mater.* **2001**, *13*, 943.
(22) Du Pasquier, A.; Blyr, A.; Courjal, P.; Amatucci, G.; Gerand, B.; Tarascon, J.-M. *J. Electrochem. Soc.* **1999**, *146*, 428.
(23) Moshkovich, M.; Cojocaru, M.; Gottlieb, H. E.; Aurbach, D. *J. Electroanal. Chem.* **2001**, *497*, 84.
(24) Kanamura, K. *J. Electrochem. Soc.* **1996**, *143*, 2548.
(25) Kanamura, K. *J. Power Sources* **1999**, *81*−*82*, 123.
(26) Belanger, D.; Ren, X. M.; Davey, J.; Uribe, F.; Gottesfeld, S. *J. Electrochem. Soc.* **2000**, *147*, 2923.
(27) Rossouw, M. H.; Liles, D. C.; Thackeray, M. M. *J. Solid State Chem.* **1993**, *104*, 464.
(28) Synchrotron powder XRD experiments were carried out at the 8C2 HRPD beamline of Pohang Accelerator Laboratory (PAL). Incident X-rays were monochromatized to the wavelength of 1.5495 Å by a double bounce Si(111) monochromator.
(29) Rietveld refinement was carried out using FullProf (Rodriguez-Carvajal, J. Abstracts of the Satellite Meeting on Powder Diffraction of the XV Congress of the IUCr, Toulouse, France, 1990; p 127) software. All the reliability factors (*R*-factors) were slightly high due to the preferred orientation effect along the *c*-axis, which was observed in the XRD pattern of pristine NDs (R_p = 14.2%, R_{wp} = 18.7%, R_{exp} = 11.35%).
(30) Gao, H. X.; Jiang, T.; Han, B. X.; Wang, Y.; Du, J. M.; Liu, Z. M.; Zhang, J. L. *Polymer* **2004**, *45*, 3017.
(31) Chiou, N. R.; Epstein, A. J. *Adv. Mater.* **2005**, *17*, 1679.
(32) Pouget, J. P.; Jozefouiczz, M. E.; Epstein, A. J.; Tang, X.; MacDiarmid, X. A. G. *Macromolecules* **1991**, *24*, 779.
(33) Kosova, N. V.; Devyatkina, E. T.; Kaichev, V. V. *Inorg. Mater.* **2007**, *43*, 185.
(34) Wang, M.; Alexandra, N. *J. Solid State Chem.* **2005**, *178*, 1230.
(35) Cao, Y.; Li, S.; Xue, Z.; Guo, D. *Synth. Met.* **1986**, *16*, 305.
(36) Furukawa, Y.; Ueda, F.; Hyodo, Y.; Harada, I. *Macromolecules* **1988**, *21*, 1297.
(37) Kerr, T. A.; Wu, H.; Nazar, L. F. *Chem. Mater.* **1996**, *8*, 2005.
(38) Wu, C.-G.; DeGroot, D. C.; Marcy, H. O.; Schindler, J. L.; Kannewurf, C. R.; Liu, Y.-J.; Hirpo, W.; Kanatzidid, G. *Chem. Mater.* **1996**, *8*, 1992.
(39) Nam, H.-J.; Kim, H.; Chang, S. H.; Kang, S.-G.; Byeon, S.-H. *Solid State Ionics* **1990**, *120*, 189.
(40) Xu, P.; Han, X.; Jiang, J.; Wang, X.; Li, X.; Wen, A. *J. Phys. Chem. C* **2007**, *111*, 12603.
(41) Yin, W.; Ruckenstein, E. *Synth. Met.* **2000**, *108*, 39.
(42) Kimura, F.; Kimura, T.; Sugisaki, A.; Komatsu, M.; Sata, H.; Ito, E. *J. Polym. Sci., Part B: Polym. Phys.* **1997**, *35*, 2741.
(43) Kimura, F.; Komatsu, M.; Kimura, T. *Appl. Spectrosc.* **2000**, *54*, 974.
(44) Cleveland, C. S.; Guigley, K. S.; Painter, P. C.; Coleman, M. M. *Macromolecules* **2000**, *33*, 4278.
(45) Grohens, Y.; Brogly, M.; Labbe, C.; Schultz, J. *Polymer* **1997**, *38*, 5913.
(46) Yavuz, A. G.; Gok, A. *Synth. Met.* **2007**, *157*, 235.
(47) Mohilner, D. M.; Adams, R. N.; Argersinger, W. J., Jr. *J. Am. Chem. Soc.* **1962**, *84*, 3618.
(48) Adams, P. N.; Laughlin, P. J.; Monkman, A. P. *Polymer* **1996**, *15*, 3411.
(49) Thackeray, M. M. *Prog. Solid State Chem.* **1997**, *25*, 1.
(50) Ohzuku, T.; Ueda, A. *J. Electrochem. Soc.* **1994**, *141*, 2972.
(51) Wang, H. F.; Jang, Y. I.; Huang, B. Y.; Sadoway, D. R.; Chiang, Y. T. *J. Electrochem. Soc.* **1999**, *146*, 473.
(52) Amatucci, G. G.; Tarascon, J. M.; Klein, L. C. *Solid State Ionics* **1996**, *83*, 167.
(53) Pereira, N.; Matthias, C.; Bell, K.; Badway, F.; Plitz, I.; Al-Sharab, J.; Cosandey, F.; Shah, P.; Isaacs, N.; Amatucci, G. G. *J. Electrochem. Soc.* **2005**, *152*, A114.
(54) Park, Y. J.; Hong, Y.-S.; Wu, X.; Kim, M. G.; Ryu, K. S.; Chang, S. H. *J. Electrochem. Soc.* **2004**, *151*, A720.
(55) Lu, Z.; Beaulieu, L. Y.; Donaberger, R. A.; Thomas, C. L.; Dahn, J. R. *J. Electrochem. Soc.* **2002**, *149*, A778.
(56) Lu, Z.; Dahn, J. R. *J. Electrochem. Soc.* **2002**, *149*, A1454.

JP9095437